Bismuth-oxo clusters for next generation extreme ultraviolet light photolithography

Harvey K. MacKenzie,[1,2] Etienne A. LaPierre,[1]* Qi Zhang,[3] Oleg Kostko,[3] Harrison K. S. Young[1,2] and Ian Manners[1,2†]

[1] Department of Chemistry, University of Victoria, Victoria, British Columbia, V8P 5C2, Canada

[2] Centre for Advanced Materials and Related Technology (CAMTEC), University of Victoria, 3800 Finnerty Rd, Victoria, BC, V8P 5C2, Canada

[3] Center for X-Ray Optics, Lawrence Berkeley National Laboratory, Berkeley, CA 94720, USA

*To whom correspondence should be addressed: elapierre@uvic.ca

Abstract

Photolithography is the primary technique used for patterning of semiconducting materials for chip manufacturing; however, as requisite pattern dimensions and feature sizes continue to decrease, state-of-the-art lithographic methods now require the use of 13.5 nm extreme ultraviolet (EUV) light. The shift towards these higher energy wavelengths of light has resulted in a need for new single component materials, with high EUV absorption cross-sections and high etch resistance. Herein, we report the exploration of $Bi_9O_7(hfac)_{13}$ as the first bismuth oxo cluster based EUV photoresist. It was determined this material has an exceptional EUV linear absorption coefficient (24 μm^{-1}), nearly an order of magnitude larger than commercially available chemically amplified resists (CARs) (~ 5 μm^{-1}). Additionally, the resist was determined to be highly sensitive to EUV exposure and displayed a crosslinking dose of 10 mJ/cm^2, undergoing ligand decomposition during exposure and crosslinking during the post-exposure bake, which was supported by FTIR and residual gas analysis. This class of bismuth-oxo cluster resists can lead to the development of more efficient, effective and safe EUV resist materials required for next-generation photolithography.

Introduction

For the past 50 years, photolithography has been the primary technique used by the semiconductor industry to pattern microchips. Throughout this period Moore's law successfully projected the doubling of the number of transistors on integrated circuits every two years.[1] This benchmark has set an industrial standard and keeping pace with this prediction has driven significant innovation in the field of high-resolution photolithographic techniques.[1-3] Recent decades saw the implementation of deep ultraviolet light (DUV, 193 nm) lithography; however, as the desired pattern feature size has continued to decrease, DUV lithography has reached its physical limits.[4, 5, 6] Minimum feature size in photolithography is dictated by the wavelength of light used (λ), the numerical aperture of the lens (NA) and the processing constant (k_1) which combines factors such as illumination and the sensitivity of the lithographic resist: [4, 7, 8]

$$CD = k_1\left(\frac{\lambda}{NA}\right).$$

To achieve the high-resolution patterning required in the fabrication process for advanced chips, the use of shorter wavelengths of light, such as extreme ultraviolet light (EUV, 13.5 nm), is now necessary.[4, 7, 9] While the use of EUV light enables higher resolution patterning it also introduces challenges; particularly, materials such as chemically amplified resists (CARs) that are traditionally used in photolithographic processes are completely comprised of organic materials and are suboptimal for EUV lithography.[4, 10, 11] One key disadvantage is the inherently low EUV cross-section of 2*p* elements, notably carbon, which comprise the organic based materials of CARs, and thus results in most of the incident photons passing through the material without effecting photochemistry. [8, 11-13] Their organic composition also results in a lack of etch resistance, which limits their ability to transfer patterns to silicon substrates.[4, 8, 14] The multicomponent nature of CARs also creates additional challenges when patterning smaller feature sizes, as stochastically induced defects have a greater influence at smaller length scales.[4] Further, as pattern size decreases

CARs can also undergo pattern collapse caused by solvent induced swelling during the development step and can also experience acid blur due to chemical amplification.[11, 15, 16] To address these aforementioned issues, researchers are now exploring single component inorganic materials as EUV resists due to their large EUV atomic cross-sections, improved stochastics and greater inherent etch resistance.[17-26]

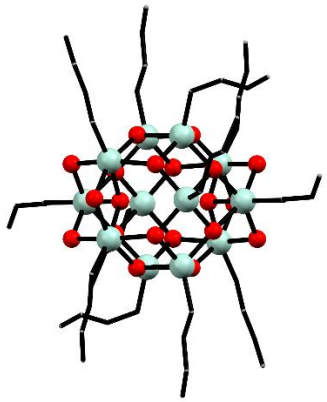

Figure 1. Molecular structure of $[(BuSn)_{12}O_{14}(OH)_6]^{2+}$ a tin oxo cluster employed as an EUV resist.[27] (red = oxygen, teal=tin)

Currently, the industry leading EUV resist materials are single component alkyl tin oxide clusters (Figure 1) that combine high EUV absorbance (~12-20 μm^{-1}), high etch resistance, and can be patterned at 8 nm half pitch with high sensitivity.[13, 27-31] While these tin oxide clusters have been extensively explored as EUV resists, there has been little success developing additional functional derivatives of this cluster framework, while the toxicity of tin-alkyls is a safety concern.[17, 32] In comparison, bismuth has a similarly high EUV absorbance cross-section to tin, is non-toxic, inexpensive, and exhibits a diverse range of coordination chemistries, which has allowed for the synthesis of numerous well-defined bismuth clusters; however, it is relatively unexplored as a component in photoresists.[33-38] Accordingly, we set out to establish the potential utility of bismuth-oxo clusters as photoresists for EUV lithography.

Results and Discussion

To investigate bismuth clusters as potential EUV photoresist candidates, the known bismuth hexafluoroacetylacetonate (hfac) cluster $Bi_9O_7(hfac)_{13}$ (**1**), was examined due to its numerous attractive properties for photoresist applications.[34] Firstly, **1** is soluble in many common coordinating solvents (tetrahydrofuran, isopropanol, acetone etc.), allowing for both a range of potential conditions necessary for thin film fabrication via spin coating and several options as resist developers. Secondly, the fluorinated hfac ligands and dense packing (2.8 $g \cdot cm^{-3}$)[34] should serve to increase the EUV absorption cross-section of the resist compared to that of organic resists.[4, 13] Lastly, the synthesis of **1** is facile, performed in a one-pot reaction, and yields spectroscopically pure material on gram scale (Figure 2).[34]

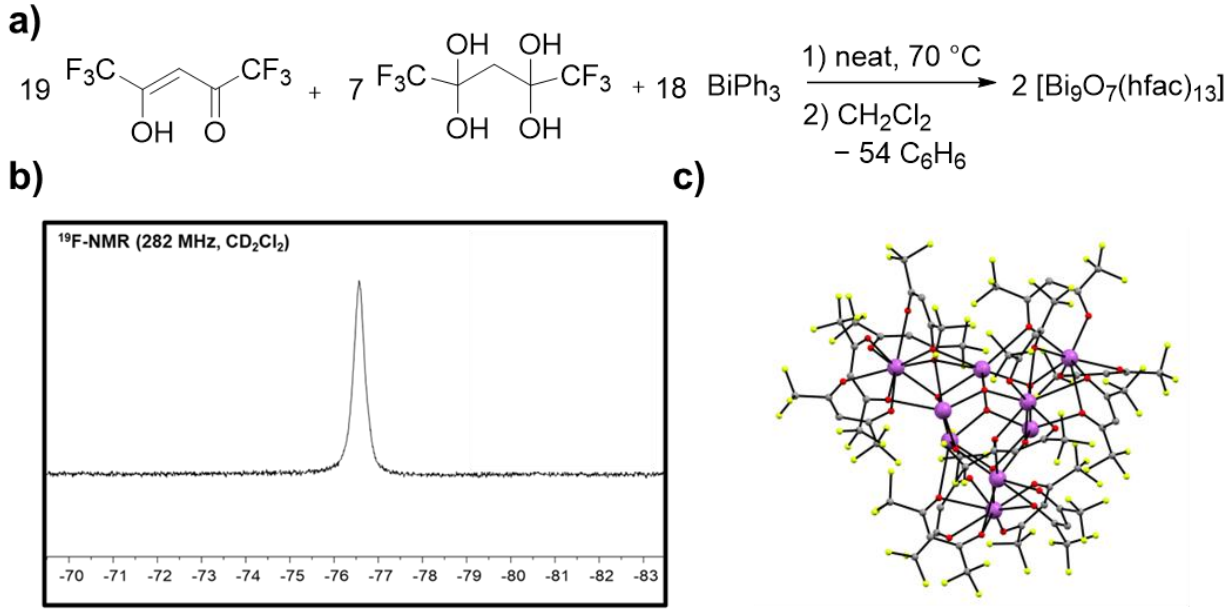

Figure 2. (a) Synthesis of $Bi_9O_7(hfac)_{13}$ (**1**); (b) ^{19}F NMR of **1**; (c) molecular structure of **1**.[34]

Fabrication of thin films of **1** on silicon wafers was achieved by spin coating **1** from isopropanol solutions of varying concentrations. 20 nm thick films could be obtained by spin coating a 15 mg/ml solution, as determined by variable angle spectroscopic ellipsometry (VASE). Such films

could be dissolved from the wafer using isopropanol, cyclohexanone, 2-heptanone and ethyl acetate, as confirmed by VASE. With films of **1** in hand, EUV absorption and photoemission properties were then explored. The EUV linear attenuation of **1** was determined using EUV reflectivity method to be 24.3 μm^{-1} (Figure S1), markedly higher than commercially available tin-oxo resists (~12-20 μm^{-1}) and nearly an order of magnitude larger than polyhydroxystyrene (PHS) based resists (~ 5 μm^{-1}).[13, 30, 39, 40] To gain further insight into the EUV absorption features of **1**, photoelectron spectroscopy (PES) was used to interrogate electron binding energies of this system upon exposure to EUV light.[41] The resulting PES spectra of **1** and PHS display stark differences, with the spectrum of **1** containing peaks at binding energies (BE) between 16-23 eV attributable to the fluorine present in the hfac ligands, and a large doublet between 34-39 eV due to emission of bismuth 5d electrons, both absent in the PHS spectrum (Figure S2). Contrastingly, in the case of PHS EUV absorption leads only to emission of valence electrons, in the case of **1** it leads to comparably strong emission of valence and Bi 5d semi-core electrons. Intensity of photoemission peaks correlates with photoabsorption cross-sections and demonstrates the difference in the absorption cross-sections between the two materials. Inelastic scattering of photoelectrons leads to emission of slow secondary electrons (with kinetic energy below 20 eV), which dominate the photoelectron spectra (Figure S2) and play significant role in solubility switch of both CAR and tin-oxide resists.[42-46] Yield of those electrons is several times higher for **1** than for PHS (Figure S2). Additionally, the total electron yield produced for **1** was determined to be 2.35 compared to a value of 0.76 for PHS (Table S1). Given these promising EUV absorptivity properties, the performance of **1** as an EUV photoresist was explored.

First, to determine the solubility switch response of **1**, EUV contrast curves were generated to interrogate resist sensitivity. Contrast curves are generated by exposing the resist at different doses, the resist is then developed and the remaining thickness of the resist is determined at each dose, these thickness are then plotted as a function of dose.[47, 48] The use of EUV contrast curves also enabled the optimization of processing protocols such as post-application bake (PAB), post-exposure bake (PEB) and development conditions for maximum EUV dose sensitivity (Figure 3).

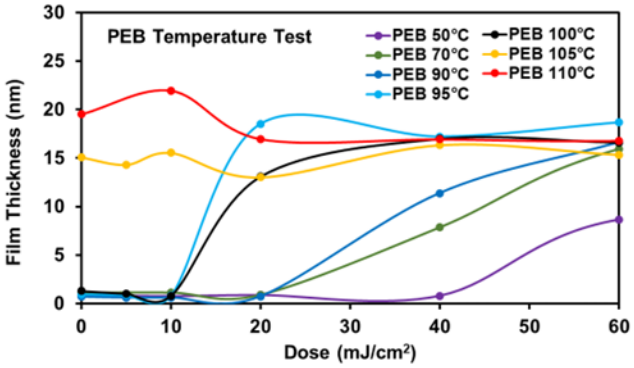

Figure 3. EUV contrast curves of **1** at various post exposure bake temperatures (50-110°C) developed with cyclohexanone.

First, **1** was aged in isopropanol for approximately 3h prior to spin coating, the film was then baked at 90 °C for 30 seconds and exposed at various doses of EUV light. After exposure, the film was then baked at 95 °C for 1 minute and developed for 30 seconds with cyclohexanone followed by a cyclohexanone rinse. The resulting contrast curve acquired under these optimized conditions indicate high sensitivity, with a dose-to-gel occurring at 10 mJ/cm^2, comparable to Inpria's commercially available tin oxo resist. [29, 49] At the dose-to-gel onset between 10 to 14 mJ/cm^2, a sharp increase in film thickness occurs (Figure 4a and S3).

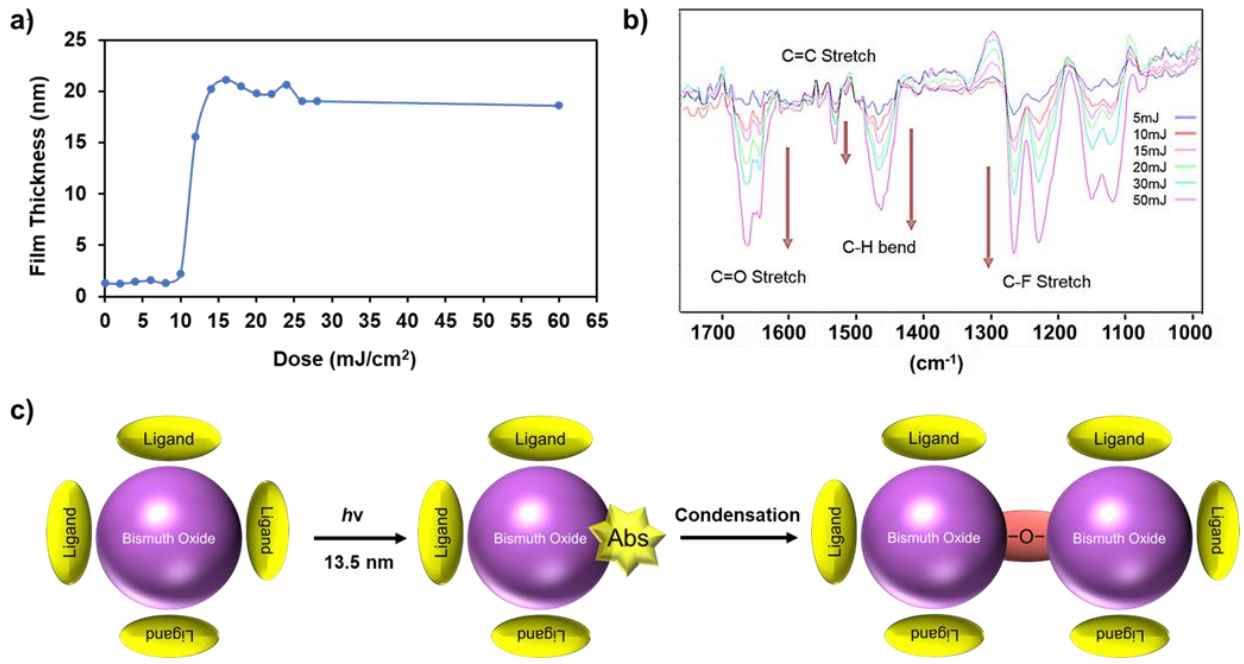

Figure 4. a) EUV contrast curve of 1, acquired using optimized conditions. b) FTIR spectra of a film of 1 at various EUV exposure doses clearly showing a reduction in hfac ligand content. c) Simplified mechanistic proposal for solubility switch chemistry of 1.

To further investigate the mechanism of the observed solubility switch, films of **1** were exposed to an electron beam (e-beam) with a kinetic energy of 20, 50 or 80 eV, at doses of 400, 800, or 1200 μC/cm^2, respectively, and residual gas analysis (RGA) was performed to determine the identity of products outgassed from the resist (Figures S4). In all cases, signals at 69 m/z (CF_3^+), 43 m/z (Scheme S1, product **A**), and 119 m/z (Scheme S1, product **B**) were present, consistent with the known electron impact ionization mass spectrum of hexafluoroacetylacetone.[50] Additionally, analysis of the films by Fourier transform infrared (FTIR) spectroscopy before and after electron beam exposure revealed a reduction in intensity of both the C=O stretching frequency at 1642 cm^{-1} and the C-F stretches between 1250 cm^{-1} and 1150 cm^{-1}, consistent with

decomposition of the hfac ligand (Figure S5). It is notable that to detect significant ligand decomposition, a high electron beam dose is required (80 eV and 1200 μC/cm^2).

For EUV exposure on films of **1**, a similar trend was observed, with FTIR revealing that ligand decomposition increased with dose, as indicated by the reduction in signals associated with the hfac ligand; most notably the C=O stretch at 1645 cm^{-1} and C-F stretches at 1262 cm^{-1} and 1218 cm^{-1} (Figure 4b). Furthermore, X-ray photoelectron spectroscopy (XPS) data comparing the original as coated film to an exposed and developed film revealed a notable decrease in fluorine content, from 36.4% fluorine to 18.3% fluorine, consistent with large amounts of ligand decomposition and loss. One plausible pathway for the decomposition of hfac is through a C-F bond activation process which occurs after ionization from an incoming EUV photon and results in Bi-F bond formation (Scheme S1) analogous to decomposition mechanisms that have been proposed in other hfac coordination compound systems ionized by laser pulses.[51-55] It was also observed that the solubility switch was heavily influenced by PEB temperature as exposed films displayed higher onset of insolubility doses at PEB temperatures lower than 95 °C (Figure S6) suggesting that the observed solubility switch chemistry is promoted by the PEB. Accordingly, we propose that the solubility switch mechanism is similar to that of Inpria's MOx and other cluster resists whereby EUV exposure triggers ligand decomposition and the resist undergoes cluster condensation during the PEB (Figure 4c).[29, 56]

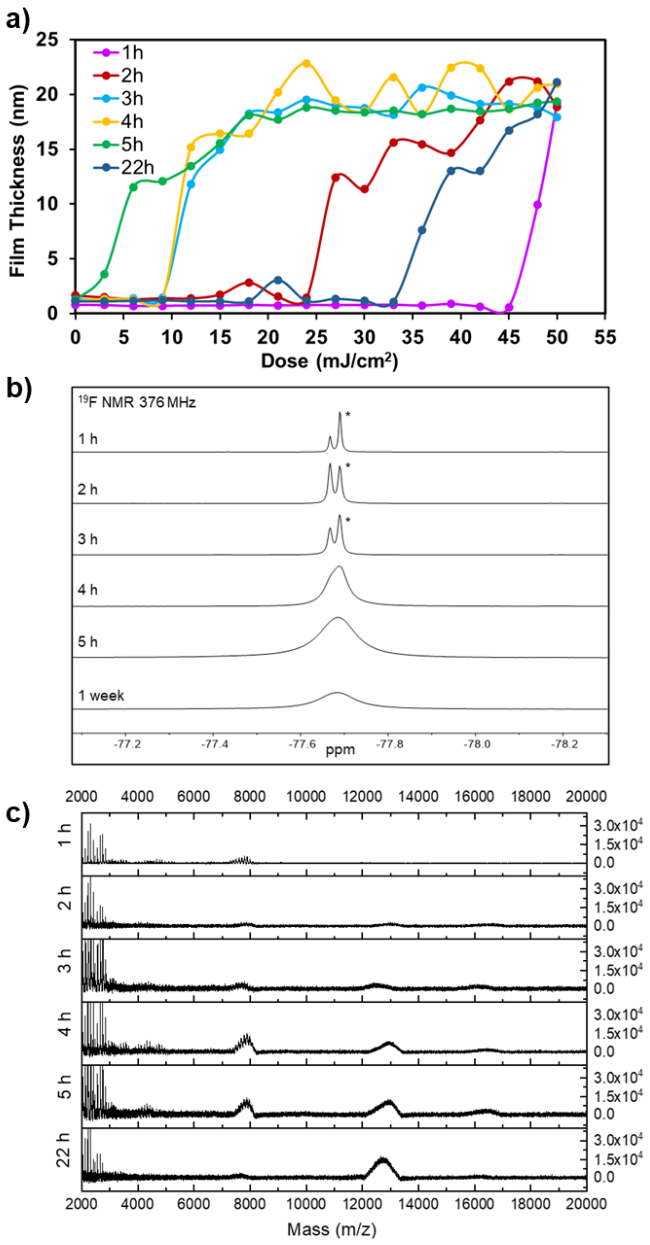

Figure 5. a) EUV contrast curves of 1 at various aging times b) ^{19}F NMR spectra of 1 at various aging times in isopropanol c) MALDI-TOF mass spectra of 1 at various aging times.

Unfortunately, attempts at further contrast curve experiments revealed considerable batch-to-batch variability. Careful examination of the experimental conditions revealed slight variation in the

solution aging times (ca. 1-3h). As previous reports indicate that **1** exhibits dynamic behavior in solution, particularly in polar solvents, leading to the eventual formation of the larger cluster $Bi_{38}O_{45}(hfac)_{24}$ (**2**) over 7 days,[34] (Figure S6), the influence of solution aging was investigated in detail. Films of **1** were cast from an isopropanol solution (**1**, 15 mg /mL), after solution aging for 1, 2, 3, 4, 5, 22 or 168 h (Figure 5a and S8). EUV contrast curves of the resulting films revealed that the insolubility onset dose for the bismuth clusters was heavily influenced by solution aging time. As aging time increases from 1 h to 4 h, the EUV dose required to induce a solubility switch decreases from approximately 50 mJ/cm^2 to 10 mJ/cm^2, with further aging to 5h resulting in a dose -to-gel below 2.5 mJ/cm^2. However, after aging the cluster solution further overnight (22 h) sensitivity significantly decreases to approximately 40 mJ/cm^2 (Figure 5a). This dramatic change in sensitivity suggests that there are significant changes occurring in the material as it is aged in solution and suggests a more rapid cluster aggregation process than the originally reported seven days.[34]

To investigate the cluster speciation in solution, an aliquot was taken from the stock solution (15 mg/mL in isopropanol) at corresponding time intervals and analyzed by $^{19}F\{^1H\}$ NMR spectrometry (Figure 5b). Upon aging for one hour, two resonances were observed in the $^{19}F\{^1H\}$ NMR spectrum, which may be attributed to the hfac ligand bound to the cluster core (−77.65 ppm) and $Bi(hfac)_3$ (−77.70 ppm).[34] As the cluster undergoes further solution aging, the two signals coalesce and broaden into a single resonance at δ_{19F} = −77.62 ppm ($\nu_{1/2}$ = 37.5 Hz) , which is suggestive of a facile rearrangement process, however, gives little information on the speciation.

To further investigate the cluster aggregation process and to identify reactive cluster species, MALDI-TOF experiments were performed at various solution aging times between 1 and 22h

(Figure 5c). Measurements of cluster solutions aged from 1 to 5 hours revealed the presence of several previously unobserved cluster sizes, as evidenced by the broad signals around m/z = 7900 and m/z = 16250. These intermediate cluster sizes then eventually coalesce to exclusively yield the $Bi_{38}O_{45}(hfac)_{24}$ (**2**) (m/z = 12800) after 22h in solution, as evidenced by MALDI-TOF mass spectrometry (Figure 5c). Additionally, the observable spacing of m/z 91 in all MALDI-TOF mass spectra arising from the aggregation of **1** can be assigned to loss of fragmentation product **C** (Scheme S1). [51, 53]

The dramatic change in EUV solubility switch sensitivity coupled with the evidence for rapid cluster aggregation suggests that there are more responsive transient cluster sizes between the two cluster sizes of Bi_9O_7 (**1**) and $Bi_{38}O_{45}$ (**2**) that were reported by Dikarev and coworkers (Scheme 1).[34] From the corresponding MALDI mass spectrometry experiments it appears that the transient cluster species which emerge from 3 to 5 hours (m/z ~ 7900 or 16250) are the reactive cluster species. Previous reports have described dynamic aggregation processes in bismuth oxide clusters, and suggest that Bi_9O_7 and $Bi_{38}O_{45}$ are "magic-size" cluster species that form in solution, representing local energy minima.[57] It is possible that in the case of **1**, spin coating from solution before full conversion to **2**, kinetically traps these transient cluster sizes, leading to the observed changes in EUV solubility switch sensitivity.[57]

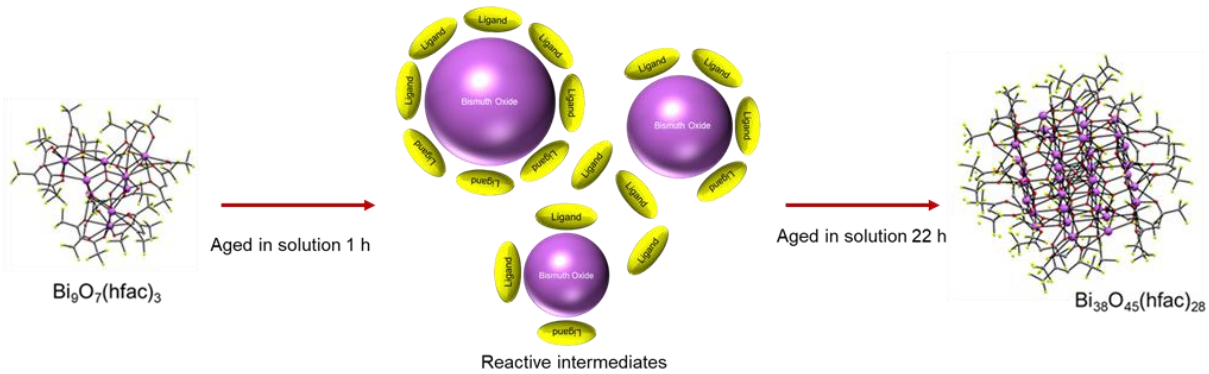

Scheme 1. Cluster aggregation process of 1 resulting in the formation of 2.

Preliminary patterning tests were performed using electron-beam (e-beam) exposure, on films of **1**. The e-beam dose-to-gel was determined to be 1370 μC/cm^2 at 100 keV, and rectangular patterns (0.5 μm × 2.5 μm) were produced (Figure S7). Other examples of metal resists have been explored for e-beam patterning have widely variable e-beam sensitivities; for example, tin oxo cluster resists were shown to have a sensitivity of 2 μC/cm^2 at 2 keV , and zinc-imidazolate resists a sensitivity of 37 mC/cm^2 at 30 keV.[58] Due to the large differences between electron beam and EUV exposure, it is difficult to use e-beam patterning as a proxy for EUV in the case of **1**, efforts to pattern these materials with EUV exposure will be explored in future studies.

Conclusions

In summary, we present the first use of a bismuth oxo cluster as an EUV photoresist, demonstrating potential as a class of inorganic resist materials. The hfac ligated bismuth-oxide cluster **1** displays a large EUV linear absorption coefficient of 24 μm^{-1} and high solubility switch sensitivity with an EUV-induced solubility switch dose of 10 mJ/cm^2, a value greater than commercially available resists, which suggest that bismuth cluster materials can exhibit competitive, if not superior, EUV response to state-of-the-art tin-oxo resists. Further investigations of **1** revealed that the sensitivity of the EUV-induced solubility switch was heavily influenced by solution aging time. Analysis of the cluster solution aging process was performed, which revealed rapid cluster aggregation and the presence of several transient clusters that could explain the solution aging-dependent solubility switch sensitivity trends observed for **1**. EUV patterning experiments utilizing this system are currently ongoing and the investigation of other bismuth cluster compounds with enhanced solution stability will be explored as resist materials in future studies.

EXPERIMENTAL SECTION

Film Fabrication

First, 1 was dissolved in isopropanol to make a 15 mg/mL solution. The solution was then sonicated for 15 minutes and filtered through a 0.2 μm PTFE syringe filter prior to spin coating. To fabricate films 1.5 mL aliquot of was dispensed onto a polished 8" silicon wafer and spun at 1500 rpm for 1 minute. The wafer was then baked at 90 °C for 30 seconds to remove residual solvent.

EUV Post Exposure Bake Optimization

A film of 1 was exposed with various doses of EUV light, between 0-60 mJ/cm^2, at spatially confined spots on the films on one quarter of the wafer. The wafer was then cleaved into 4 equal parts each containing 6 doses (0, 5, 10, 20, 40 and 60 mJ/cm^2). Each quarter of the wafer was then baked at different temperatures (90, 95, 100 and 105 °C) for 1 minute. The films were developed by placing them in the spin coater and immediately dispensing cyclohexanone to cover the entire film for 30 seconds, after which the cyclohexanone was spun off at 1500 rpm for 1 minute. After the film was developed the thickness of the film at dose spots were measured using variable angle ellipsometry and plotted as a function of EUV dose.

EUV Contrast Curves Optimized Conditions

Films of 1 (see film fabrication conditions above) were exposed with various doses of EUV light, between 0-100 mJ/cm^2, at spatially confined spots on the films. The exposed films were then subjected to a bake of 95 °C for 1 minute. The films were developed by placing them in the spin coater and immediately dispensing cyclohexanone to cover the entire film for 30 seconds, after which the cyclohexanone was removed by spinning at 1500 rpm for 1 minute, after the first 10 seconds of spinning at 1500 rpm a 5 mL cyclohexanone rinse was added to the spin coater in one shot via a syringe to ensure full removal of unexposed resist. After the film was developed the

thickness of dose spots were measured using variable angle ellipsometry and plotted as a function of EUV dose.

Solution Aging Experiment

1 was dissolved in isopropanol to make a 15 mg/mL solution. The solution was then sonicated for 15 minutes and filtered through a 0.2 μm PTFE syringe filter prior to spin coating. A 2 mL aliquot was removed at 1 hour time intervals from 0 to 5h and another at 22h. 0.5 mL of each aliquot was then added to 0.5mL of d-MeOH and mixed and a 19F NMR was taken (Figure 5b). The remaining 1.5 mL was dispensed immediately on onto a polished 8" silicon wafer and spun at 1500 rpm for 1 minute. The wafer was then baked at 90 °C for 30 seconds to remove residual solvent. An EUV contrast curve was performed with doses starting at 0 mJ/cm^2 with 3 mJ/cm^2 intervals up to 50 mJ/cm^2 (Figure 5a).

Outgassing Analysis during E-Beam Exposure and FTIR

9 spots on a thin film of 1 were exposed to electrons with kinetic energies of 20, 50, and 80 eV at three different doses: 400, 800, and 1200 $\mu C/cm^2$. Residual Gas Analysis (RGA) mass spectra of outgassed species were collected during exposure. The experimental setup included a residual gas analyzer (Stanford Research Systems Inc.) detecting mass-to-charge ratios (m/z) from 1 to 200. Background signals, recorded in the absence of electron exposure for 120 s before and after measurements, were subtracted from the outgassing signals to isolate species released from the resist during electron exposure. The resulting outgassing spectra enabled the identification of specific chemical species and the tracking of their evolution over exposure time. Mass spectra were obtained by averaging the first 40 s of signal collected during e-beam exposure. FTIR measurements of electron-exposed samples were performed in transmission geometry using a Thermo Nicolet 6700 spectrometer. Prior to data collection, samples were purged with N_2 gas to

eliminate gaseous CO_2 and water contamination. A typical measurement involves collecting a background spectrum from an unexposed film area and a signal spectrum from exposed spots. The resulting difference FTIR spectra reveal chemical changes in the film induced by electron irradiation.

EUV linear attenuation experiment

EUV absorption measurements were conducted at the Advanced Light Source (ALS) beamline 6.3.2 at Lawrence Berkeley National Laboratory using the reflectivity method.3 Reflectivity measurements at 13.5 nm were performed with a 200 mm^{-1} grating, a Be filter, and a photodiode detector. Fitting the experimental data shown in Figure S1, enabled the determination of the components of the complex refractive index. The absorptive component of the refractive index was then converted into the linear attenuation coefficient.

Photoelectron Spectroscopy

A custom-built photoelectron spectrometer (PES) at ALS beamline 12.0.1.2 was used to collect photoelectron spectra. During measurements, the sample is exposed to EUV radiation, and emitted electrons are analyzed using a retarding field analyzer. To mitigate EUV-induced changes, the instrument continuously moves the sample in front of the detector, ensuring that photoelectron signals are collected from fresh, unexposed regions of the film. This approach is crucial to minimize the material's EUV exposure during analysis. The estimated EUV dose per measurement is approximately 2 mJ/cm^2, which is generally below the sensitivity threshold of known EUV resists. The binding energy is determined in respect to vacuum level.

ASSOCIATED CONTENT

Supporting Information

The Supporting Information is available free of charge on the ACS Publications website. Experimental details and characterization, including spectroscopic data, and supplementary figures. (PDF)

AUTHOR INFORMATION

Corresponding Authors

*elapierre@uvic.ca

ORCID

Harvey K. MacKenzie: 0000-0003-2078-6998
Etienne A. LaPierre: 0000-0002-3244-3637
Qi Zhang: 0000-0002-2915-7605
Oleg Kostko: 0000-0003-2068-4991
Harrison K.S. Young: 0000-0002-3574-3950
Ian Manners: 0000-0002-3794-967X

Notes

The authors declare no competing financial interests.

†Ian Manners: Deceased December 3rd, 2023

ACKNOWLEDGMENTS

The authors thank Intel Corp for funding through the Center for Imag(in)ing New EUV Materials Architecture (CINEMA) program. Dr. James M. Blackwell (Intel Corp) is acknowledged for contributions and guidance through the CINEMA program. I.M. thanks the Canadian Government for a Canada 150 Research Chair, NSERC for a Discovery Grant, and the University of Victoria for start-up funds. E.L. thanks NSERC for a Postdoctoral Fellowship. H.K.M thanks NSERC for a CGS-D fellowship, the University of Victoria for a President's research scholarship and Intel Corp for an industrial internship. This research used resources of the Advanced Light Source, a U.S. DOE Office of Science User Facility (Grant No. DE-AC02-05CH11231).

References

(1) Mack, C. A. Fifty Years of Moore's Law. *IEEE Trans. Semicond. Manuf.* **2011**, *24* (2), 202-207.
(2) Wallraff, G. M.; Allen, R. D.; Hinsberg, W. D.; Larson, C. F.; Johnson, R. D.; DiPietro, R.; Breyta, G.; Hacker, N.; Kunz, R. R. Single-layer chemically amplified photoresists for 193-nm lithography. *J. Vac. Sci. Technol. B* **1993**, *11* (6), 2783-2788.
(3) Allen, R. D.; Wallraff, G. M.; Hofer, D. C.; Kunz, R. R. Photoresists for 193-nm lithography. *IBM J. Res. Dev.* **1997**, *41* (1.2), 95-104.
(4) Li, L.; Liu, X.; Pal, S.; Wang, S.; Ober, C. K.; Giannelis, E. P. Extreme ultraviolet resist materials for sub-7 nm patterning. *Chem. Soc. Rev.* **2017**, *46* (16), 4855-4866.
(5) Song, J.; Han, G. W.; Kim, J.; Lee, G. W. 19-nm critical dimension process using mask shift double exposure in ArF immersion. *J. Micro/Nanopatterning Mater. Metrol.* **2024**, *23* (1), 014801.
(6) Sanders, D. P. Advances in patterning materials for 193 nm immersion lithography. *Chem. Rev.* **2010**, *110* (1), 321-360.
(7) Wagner, C.; Harned, N. EUV LITHOGRAPHY Lithography gets extreme. *Nat. Photonics* **2010**, *4* (1), 24-26.
(8) Manouras, T.; Argitis, P. High Sensitivity Resists for EUV Lithography: A Review of Material Design Strategies and Performance Results. *Nanomaterials* **2020**, *10* (8), 1593.
(9) Itani, T.; Kozawa, T. Resist materials and processes for extreme ultraviolet lithography. *Jpn. J. Appl. Phys.* **2012**, *52* (1R), 010002.
(10) Ober, C. K.; Käfer, F.; Yuan, C. Y. Recent developments in photoresists for extreme-ultraviolet lithography. *Polymer* **2023**, *280*, 126020.
(11) Thackeray, J. W. Materials challenges for sub-20-nm lithography. *J. Micro/ Nanolithogr. MEMS MOEMS* **2011**, *10* (3), 033009.
(12) Closser, K. D.; Ogletree, D. F.; Naulleau, P.; Prendergast, D. The importance of inner-shell electronic structure for enhancing the EUV absorption of photoresist materials. *J. Chem. Phys.* **2017**, *146* (16), 164106.
(13) Fallica, R.; Stowers, J.; Grenville, A.; Frommhold, A.; Robinson, A.; Ekinci, Y. *Dynamic absorption coefficients of CAR and non-CAR resists at EUV*; SPIE, 2016.
(14) Ober, C.; Xu, H.; Kosma, V.; Sakai, K.; Giannelis, E. *EUV photolithography: resist progress and challenges*; SPIE, 2018.
(15) Chini, S. F.; Amirfazli, A. Understanding pattern collapse in photolithography process due to capillary forces. *Langmuir* **2010**, *26* (16), 13707-13714.
(16) Lee, H.; Park, S.; Kim, M.; Moon, J.; Lee, B.; Cho, M. Multiscale simulation of extreme ultraviolet nanolithography: impact of acid–base reaction on pattern roughness. *J. Mat. Chem. C* **2021**, *9* (4), 1183-1195, 10.1039/D0TC04104A.
(17) Cardineau, B.; Del Re, R.; Marnell, M.; Al-Mashat, H.; Vockenhuber, M.; Ekinci, Y.; Sarma, C.; Freedman, D. A.; Brainard, R. L. Photolithographic properties of tin-oxo clusters using extreme ultraviolet light (13.5nm). *Microelectron. Eng.* **2014**, *127*, 44-50.
(18) Luo, C.; Xu, C.; Lv, L.; Li, H.; Huang, X.; Liu, W. Review of recent advances in inorganic photoresists. *RSC Adv.* **2020**, *10* (14), 8385-8395.
(19) Lim, G.; Lee, K.; Koh, C.; Nishi, T.; Yoon, H. J. Multinuclear Tin-Based Macrocyclic Organometallic Resist for EUV Photolithography. *ACS Mater. Au* **2024**, *4* (5), 468-478.

(20) Thakur, N.; Tseng, L. T.; Vockenhuber, M.; Ekinci, Y.; Castellanos, S. Stability studies on a sensitive EUV photoresist based on zinc metal oxoclusters. *J. Micro/ Nanolithogr. MEMS MOEMS* **2019**, *18* (4), 043504-043504.
(21) Tseng, Y.-F.; Liao, P.-C.; Chen, P.-H.; Gau, T.-S.; Lin, B.-J.; Chiu, P.-W.; Liu, J.-H. Highly hydroxylated hafnium clusters are accessible to high resolution EUV photoresists under small energy doses. *Nanoscale Adv.* **2024**, *6* (1), 197-208.
(22) Wu, J. R.; Lin, T. A.; Wu, Y. R.; Chen, P. H.; Gau, T. S.; Lin, B. J.; Chiu, P. W.; Liu, R. S. Novel hexameric tin carboxylate clusters as efficient negative-tone EUV photoresists: high resolution with well-defined patterns under low energy doses. *Nanoscale Adv.* **2023**, *5* (11), 3033-3043.
(23) Lim, G.; Lee, K.; Choi, S.; Yoon, H. J. Organometallic and coordinative photoresist materials for EUV lithography and related photolytic mechanisms. *Coord. Chem. Rev.* **2023**, *493*, 215307.
(24) Fallica, R.; Haitjema, J.; Wu, L.; Castellanos, S.; Brouwer, A. M.; Ekinci, Y. Absorption coefficient of metal-containing photoresists in the extreme ultraviolet. *J. Micro/ Nanolithogr. MEMS MOEMS* **2018**, *17* (2), 023505.
(25) Evrard, Q.; Sadegh, N.; Mathew, S.; Zuidinga, E.; Watts, B.; Paradiz Dominguez, M.; Giglia, A.; Mahne, N.; Nannarone, S.; Nishimura, A.; Goya, T.; Sugioka, T.; Vockenhuber.; Ekinici, Y.; Brouwer, A. M. Extreme Ultraviolet Photoresponse of Organotin-Based Photoresists with Borate Counteranions. *ACS Appl. Mater. Interfaces* **2024**, *16* (32), 42947-42956.
(26) Liu, F. F.; Shi, G. Y.; Zhen, N.; Zhou, Z. H.; Guo, T. L.; Qiao, Y.; Zhao, J.; Liu, J. C.; Luo, F.; Zhang, L. Single Rare-Earth Ion Doped Tin-Oxo Nanocluster Photoresists for High-Resolution Extreme Ultraviolet Lithography. *Nano Lett.* **2025**, *25* (5), 2067-2073.
(27) Eychenne-Baron, C.; Ribot, F.; Steunou, N.; Sanchez, C.; Fayon, F.; Biesemans, M.; Martins, J. C.; Willem, R. Reaction of butyltin hydroxide oxide with p-toluenesulfonic acid:: Synthesis, X-ray crystal analysis, and multinuclear NMR characterization of {(BuSn)O(OH)}(4-CHCHSO). *Organometallics* **2000**, *19* (10), 1940-1949.
(28) Ma, J. H.; Needham, C.; Wang, H.; Neureuther, A.; Prendergast, D.; Naulleau, P. Mechanistic Advantages of Organotin Molecular EUV Photoresists. *ACS Appl. Mater. Interfaces* **2022**, *14* (4), 5514-5524.
(29) Hinsberg, W. D.; Meyers, S. A numeric model for the imaging mechanism of metal oxide EUV resists. In *Advances in Patterning Materials and Processes XXXIV*, 2017; SPIE: Vol. 10146, pp 14-24.
(30) Grenville, A.; Anderson, J. T.; Clark, B. L.; De Schepper, P.; Edson, J.; Greer, M.; Jiang, K.; Kocsis, M.; Meyers, S. T.; Stowers, J. K.; Telecky, A. J.; De Simone, D.; Vandenberghe, G. Integrated fab process for metal oxide EUV photoresist. 2015, SPIE.
(31) Anderson, C.; Allezy, A.; Chao, W.; Conley, L.; Cork, C.; Cork, W.; Delano, R.; DePonte, J.; Dickinson, M.; Gaines, G. How we are making the 0.5-NA Berkeley mirco-field exposure tool stable and productive. In *Extreme Ultraviolet (EUV) Lithography XI*, 2020; SPIE: Vol. 11323, pp 48-55.
(32) Rudel, H. Case study: bioavailability of tin and tin compounds. *Ecotoxicol. Environ. Saf.* **2003**, *56* (1), 180-189.
(33) Mansfeld, D.; Mehring, M.; Schurmann, M. From a monomeric bismuth silanolate to a molecular bismuth oxo cluster: [Bi22O26(OSiMe2tBu)14]. *Angew. Chem. Int. Ed.* **2004**, *44* (2), 245-249.

(34) Dikarev, E. V.; Zhang, H.; Li, B. From a bismuth oxido diketonate to a giant bismuth oxido cluster. *Angew. Chem. Int. Ed.* **2006**, *45* (33), 5448-5451.
(35) Andrews, P. C.; Deacon, G. B.; Forsyth, C. M.; Junk, P. C.; Kumar, I.; Maguire, M. Towards a structural understanding of the anti-ulcer and anti-gastritis drug bismuth subsalicylate. *Angew. Chem. Int. Ed.* **2006**, *45* (34), 5638-5642.
(36) Mehring, M. From molecules to bismuth oxide-based materials: Potential homo- and heterometallic precursors and model compounds. *Coord. Chem. Rev.* **2007**, *251* (7-8), 974-1006.
(37) Passarelli, J.; Sortland, M.; Del Re, R.; Cardineau, B.; Sarma, C.; Freedman, D. A.; Brainard, R. L. Bismuth Resists for EUV Lithography. *J. Photopolym. Sci. Technol.* **2014**, *27* (5), 655-661.
(38) Whitmire, K. H.; Wall, K. The oxido clusters of bismuth. *Coord. Chem. Rev.* **2023**, *488*, 215072.
(39) Kozawa, T.; Okamoto, K.; Nakamura, J.; Tagawa, S. Feasibility study on high-sensitivity chemically amplified resist by polymer absorption enhancement in extreme ultraviolet lithography. *Appl. Phys. Express* **2008**, *1* (6), 067012.
(40) Hirose, R.; Kozawa, T.; Tagawa, S.; Kai, T.; Shimokawa, T. Dependence of absorption coefficient and acid generation efficiency on acid generator concentration in chemically amplified resist for extreme ultraviolet lithography. *Jpn. J. Appl. Phys.Part 2* **2007**, *46* (36-40), L979-L981.
(41) Kostko, O.; McAfee, T.; Naulleau, P. *Experimental characterization of EUV resist materials: photoelectron spectroscopy*; SPIE, 2022.
(42) Hinsberg, W.; Meyers, S. *A numeric model for the imaging mechanism of metal oxide EUV resists*; SPIE, 2017.
(43) Zhang, Y.; Haitjema, J.; Liu, X.; Johansson, F.; Lindblad, A.; Castellanos, S.; Ottosson, N.; Brouwer, A. M. Photochemical conversion of tin-oxo cage compounds studied using hard x-ray photoelectron spectroscopy. *J. Micro/ Nanolithogr. MEMS MOEMS* **2017**, *16* (2), 023510-023510.
(44) Bespalov, I.; Zhang, Y.; Haitjema, J.; Tromp, R. M.; van der Molen, S. J.; Brouwer, A. M.; Jobst, J.; Castellanos, S. Key Role of Very Low Energy Electrons in Tin-Based Molecular Resists for Extreme Ultraviolet Nanolithography. *ACS Appl. Mater. Interfaces* **2020**, *12* (8), 9881-9889.
(45) Hinsberg, W.; Wallraff, G. Lithographic resists. *Encyclopedia of Polymer Science and Technology* **2002**.
(46) Kozawa, T.; Tagawa, S. Radiation Chemistry in Chemically Amplified Resists. *Jpn. J. Appl. Phys.* **2010**, *49* (3), 030001.
(47) Deng, J.; Bailey, S.; Jiang, S.; Ober, C. K. Modular Synthesis of Phthalaldehyde Derivatives Enabling Access to Photoacid Generator-Bound Self-Immolative Polymer Resists with Next-Generation Photolithographic Properties. *J. Am. Chem. Soc.* **2022**, *144* (42), 19508-19520.
(48) Levinson, H. J. *Principles of lithography*; SPIE press, 2005.
(49) Haitjema, J.; Zhang, Y.; Vockenhuber, M.; Kazazis, D.; Ekinci, Y.; Brouwer, A. Extreme ultraviolet patterning of tin-oxo cages. *J. Micro/ Nanolithogr. MEMS MOEMS* **2017**, *16* (3), 033510.
(50) Wallace, W. E. *"Mass Spectra" in NIST Chemistry WebBook, NIST Standard Reference Database Number 69,* ; National Institute of Standards and Technology, Gaithersburg, MD, 20899.

(51) Chen, J.; Xing, X.; Rey-de-Castro, R.; Rabitz, H. Ultrafast Photofragmentation of Ln(hfac)(3) with a Proposed Mechanism for forming High Mass Fluorinated Products. *Sci. Rep.* **2020**, *10* (1), 7066.
(52) Engmann, S.; Omarsson, B.; Lacko, M.; Stano, M.; Matejcik, S.; Ingolfsson, O. Dissociative electron attachment to hexafluoroacetylacetone and its bidentate metal complexes M(hfac)2; M = Cu, Pd. *J. Chem. Phys.* **2013**, *138* (23), 234309.
(53) Meng, Q.; Witte, R. J.; May, P. S.; Berry, M. T. Photodissociation and Photoionization Mechanisms in Lanthanide-based Fluorinated β-Diketonate Metal−Organic Chemical-Vapor Deposition Precursors. *Chem. Mater.* **2009**, *21* (24), 5801-5808.
(54) Talaga, D. S.; Hanna, S. D.; Zink, J. I. Luminescent photofragments of (1,1,1,5,5,5-hexafluoro-2,4-pentanedionato) metal complexes in the gas phase. *Inorg. Chem.* **1998**, *37* (12), 2880-2887.
(55) Condorelli, G. G.; Baeri, A.; Fragalà, I. L. Kinetics and Mechanisms of MOCVD Processes for the Fabrication of Sr-Containing Films From Sr(hfac)2Tetraglyme Precursor. *Chem. Mater.* **2002**, *14* (10), 4307-4312.
(56) Li, L.; Chakrabarty, S.; Spyrou, K.; Ober, C. K.; Giannelis, E. P. Studying the Mechanism of Hybrid Nanoparticle Photoresists: Effect of Particle Size on Photopatterning. *Chem. Mater.* **2015**, *27* (14), 5027-5031.
(57) Szczerba, D.; Tan, D.; Do, J. L.; Titi, H. M.; Mouhtadi, S.; Chaumont, D.; Del Carmen Marco de Lucas, M.; Geoffroy, N.; Meyer, M.; Rousselin, Y.; Hudspeth, J. M.; Schwanen, V.; Spoerk-Erdely, P.; Dippel, A.; Ivashko, O.; Gutowski, O.; Glaevecke, P.; Bazhenov, V.; Arhangelskis, M.; Halasz, I.; Friščić, T.; Kimber, S. A. Real-Time Observation of "Soft" Magic-Size Clusters during Hydrolysis of the Model Metallodrug Bismuth Disalicylate. *J. Am. Chem. Soc.* **2021**, *143* (40), 16332-16336.
(58) Corkery, P.; Waltz, K. E.; Eckhert, P. M.; Ahmad, M.; Kraetz, A.; Miao, Y.; Lee, D. T.; Abdel-Rahman, M. K.; Lan, Y.; Haghi-Ashtiani, P.; Stein, A.; Boscoboinik, J. A.; Tsapatsis, M.; Fairbrother, D. M. Zinc-Imidazolate Films as an All-Dry Resist Technology. *Adv. Funct. Mater.* **2023**, *34* (12), 2311149.

TOC